agents with $n_g = 32$, on networks containing 4, 6, 8 hosts, the average numbers of MGA generations required to solve the problem are 8.5, 7.4, 6.6, respectively. We observe that increasing the meta population size, the solving time is reduced.

6. Conclusions

In the paper is demonstrated the capability of the distributed evolutionary algorithms to solve the inverse ENDE problems and to reconstruct the flaws in an effective and accurate manner.

Additionally to the pre-tuning, an original hierarchical structure is proposed to realise self-adaptive evolutionary parameter control. The lower level of the software system contains "slave" evolutionary agents, structured as in the "island model" with ring communication topology. The upper level is a supervisor evolutionary agent which acts as an meta-algorithm, aiming to improve the behaviour of the EAs population. The Java mobile agent (aglet) technology used to develop the distributed software system proved to be a very effective technique to parallelise portable tasks.

Acknowledgments

The authors thank Prof. Irina Munteanu for her valuable contribution to our article improvement.

The authors acknowledge the support of Romania Ministry of Education and National Agency of Science and Technology under the grants CNCSIS/BCUM/CoLaborator and ANSTI no. 836.

References

[1] T. Takagi, H. Fukutomi. Benchmark Activities of Eddy Current Testing for Steam Generator Tubes. In *Electromagnetic Nondestructive Evaluation (IV)*, vol. 17, pp. 235–252. S.S. Udpa, T. Takagi, J. Pavo and R. Albanese (Ed). IOS Press, Amsterdam, 2000. ISBN 1 58603 023 X.

[2] D. Ioan, G. Ciuprina, C. Dumitrescu. Use of stochastic algorithms for distributed architectures in the optimization of electromagnetic devices. *IEEE Transactions on Magnetics*, vol. 34, no. 5, pp. 3000–3003, 1998.

[3] R. Albanese, G. Rubinacci, A. Tamburrino, F. Villone. Effects of Crack Thickness in Eddy Current Testing. In *Electromagnetic Nondestructive Evaluation (IV)*, vol. 17, pp. 25–31. S.S. Udpa, T. Takagi, J. Pavo and R. Albanese (Ed), IOS Press, Amsterdam, 2000. ISBN 1 58603 023 X.

[4] A.E. Eiben, R. Hinterding, Z. Michalewicz. Parameter control in evolutionary algorithms. *IEEE Trans. Evolutionary Comp.*, vol. 3, no. 2, pp. 124–141, July 1999.

[5] Z. Michalewicz. *Genetic Algorithms + Data Structures = Evolution Programs*. Springer-Verlag Berlin, 1996.

[6] D. Fogel. What is evolutionary computation? *IEEE Spectrum*, vol. 37, pp. 26–32, January 2000.

[7] D. Lange, M. Oshima. *Programming and Deploying Java Mobile Agents with Aglets*. Addison-Wesley, 1998.

Electromagnetic Nondestructive Evaluation (V)
J. Pávó et al. (Eds.)
IOS Press, 2001

Crack Reconstruction in Ferromagnetic Materials using Nonlinear FEM-BEM Scheme and Neural Networks

Ovidiu Mihalache, Gabriel Preda, Tetsuya Uchimoto, Kazuyuki Demachi and Kenzo Miya
Nuclear Engineering Research Laboratory, Graduate School of Engineering, The University of Tokyo, Tokai-mura, Naka-gun, Ibaraki 319-1106, Japan
E-mail:omih@tokai.t.u-tokyo.ac.jp

Abstract. The present paper studies the application of an NDT technique using static field for detecting defects in ferromagnetic materials. Both direct simulation of nonlinear magnetic field phenomena using a FEM-BEM code and Neural Networks-based inversion techniques are performed. Numerical results for the inversion of signals due to outer defects are shown.

1. Introduction

Eddy current testing (ECT) has been extensively used for the inspection of steam generator (SG) tubing of pressurized water nuclear reactors (PWR). Although ECT offers major advantages with regard to high speed and reliability to in-service inspection, its applicability is limited by skin effect only to thin, non-magnetic structural components. The detection and characterization of defect through inverse procedures in structural steels, including ferromagnetic materials, thick structures and welded parts raised recently the necessity of developing new techniques such as the nonlinear static field analysis. The increased ill-posedness of inverse problem of reconstruction from signals coming from static field is a major drawback of this method, although the choice of the numerical formulation ensure a good performance in terms of rapidity of the forward solver.

2. Direct problem analysis for crack detection

The simulation tool for the forward problem numerical computations involved in this paper is a 3-D code, based on a FEM-BEM formulation for magnetic vector potential **A**. From Maxwell equations in the limits of magnetostatic field, taking into account the nonlinear constitutive relationship:

$$\mathbf{H} = \mathbf{F}(\mathbf{B}), \tag{1}$$

and using the Coulomb gauge *div* **A**=0, the governing equations are obtained:

$$-\frac{1}{\mu_0}\Delta\mathbf{A} = \nabla\times\mathbf{M} \quad in\,\Omega_F, \tag{2}$$

$$-\frac{1}{\mu_0}\Delta\mathbf{A}=\mathbf{J}_0 \quad in\,\Omega_0\,, \tag{3}$$

where $\Omega = \Omega_F \cup \Omega_0$ is an unbounded domain, Ω_F is the ferromagnetic domain and Ω_0 is the air. The sources of magnetic field are the impressed current sources $\mathbf{J}_0$ in the air and the magnetization $\mathbf{M}$ inside the ferromagnetic bodies. The nonlinear media having the constitutive relationship (1) are replaced by a linear one having vacuum permeability and a magnetization iteratively corrected through a fixed point procedure based on Hantila's polarization method [1] [2]. Relation (1) is replaced by:

$$\mathbf{B}=\mu_0(\mathbf{H}+\mathbf{M})\,, \tag{4}$$

where the nonlinearity is hidden in the polarization term $\mu_0\mathbf{M}$:

$$\mathbf{M} = 1/\mu_0\,\mathbf{B}-\mathbf{F}(\mathbf{B})=\mathbf{G}(\mathbf{B}). \tag{5}$$

On the interface between the FEM-domain (magnetic material) and BEM-domain (air) the tangential component of $\mathbf{H}$ is continuous only in a weak sense [3]:

$$\left.\frac{1}{\mu_0}\frac{\partial\mathbf{A}}{\partial\mathbf{n}}-\mathbf{M}\times\mathbf{n}\right|_{FEM}=\left.\frac{1}{\mu_0}\frac{\partial\mathbf{A}}{\partial\mathbf{n}}\right|_{BEM} \tag{6}$$

3. Numerical formulation for FEM-BEM coupling

For the ferromagnetic domain Ω_F, a FEM formulation is developed. Using Galerkin approach:

$$\mathbf{A}=\sum_{j=1}^{n}N_j\mathbf{A}_j\,, \tag{7}$$

equation (2) is discretized by projecting each term of the equations on the shape functions and integrating over the entire problem domain Ω. For the term in the left hand side of equation (2) we have:

$$\int_\Omega\frac{1}{\mu_0}\Delta\mathbf{A}N_k\,d\Omega=\int_{\partial\Omega}\frac{1}{\mu_0}N_k\frac{\partial\mathbf{A}}{\partial n}d\Gamma-\int_\Omega\frac{1}{\mu_0}\nabla N_k\cdot\nabla\begin{pmatrix}A_x\\A_y\\A_z\end{pmatrix}d\Omega=$$
$$\sum_{j=1}^{n}\left(\int_{\partial\Omega}\frac{1}{\mu_0}N_kN_j\,d\Gamma\right)\begin{pmatrix}\partial A_{xj}/\partial n\\\partial A_{yj}/\partial n\\\partial A_{zj}/\partial n\end{pmatrix}-\sum_{j=1}^{n}\left(\int_\Omega\frac{1}{\mu_0}\nabla N_k\cdot\nabla N_j\,d\Omega\right)\begin{pmatrix}A_{xj}\\A_{yj}\\A_{zj}\end{pmatrix}, \tag{8}$$

with $\partial\Omega$ being the external surface of domain Ω. For the term in the right hand side of equation (2) we use a similar technique:

$$\int_\Omega(\nabla\times\mathbf{M})N_k\,d\Omega=-\int_{\partial\Omega}(\mathbf{M}\times\mathbf{n})N_k\,d\Gamma+\int_\Omega(\nabla N_k\times\mathbf{M})d\Omega\,, \tag{9}$$

The surface and volume integral from equation (9) can be written in the following way:

$$\int_{\partial\Omega}(\mathbf{M}\times\mathbf{n})N_k\,d\Gamma=\sum_{j=1}^{n}\left(\int_{\partial\Omega}N_kN_j\,d\Gamma\right)\begin{pmatrix}(\mathbf{M}_j\times\mathbf{n})_x\\(\mathbf{M}_j\times\mathbf{n})_y\\(\mathbf{M}_j\times\mathbf{n})_z\end{pmatrix} \tag{10}$$

$$\int_\Omega(\nabla N_k\times\mathbf{M})d\Omega=\sum_{j=1}^{n}\left(\int_{\omega_j}\nabla N_k\,d\Omega\right)\begin{pmatrix}\mathbf{j}\cdot\mathbf{M}_{zj}-\mathbf{k}\cdot\mathbf{M}_{yj}\\\mathbf{k}\cdot\mathbf{M}_{xj}-\mathbf{i}\cdot\mathbf{M}_{zj}\\\mathbf{i}\cdot\mathbf{M}_{yj}-\mathbf{j}\cdot\mathbf{M}_{xj}\end{pmatrix}, \tag{11}$$

with $\mathbf{i}$, $\mathbf{j}$, $\mathbf{k}$ being the versors of Cartesian system of coordinates and ω_j an hexahedral element of the mesh. The equation system obtained is:

$$\begin{bmatrix}N_1&0&0\\0&N_1&0\\0&0&N_1\end{bmatrix}\begin{Bmatrix}A_x\\A_y\\A_z\end{Bmatrix}=\begin{Bmatrix}f_x\\f_y\\f_z\end{Bmatrix}+\begin{Bmatrix}f_{Mx}\\f_{My}\\f_{Mz}\end{Bmatrix}, \tag{12}$$

or, after assembling the system matrix for *FEM*:

$$[\mathbf{P}]\{\mathbf{A}\}+=\{\mathbf{f}\}+\{\mathbf{f_M}\}, \tag{13}$$

with $\{f\}=[D]\{\partial A/\partial n\}+[D]\mu_0\{\mathbf{M}\times\mathbf{n}\}$ where [D] is the distribution matrix.

Here, elements of [P] and [D] matrices are:

$$N_{1kj}=\int_\Omega\frac{1}{\mu_0}\nabla N_k\cdot\nabla N_j\,d\Omega,\quad D_{kj}=\int_\Gamma\frac{1}{\mu_0}N_kN_j\,d\Gamma,\quad k=1,n,\ j=1,n\,, \tag{14}$$

with n being the number of nodes in the *FEM* domain.

For the air domain Ω_0, the boundary element method (BEM) is used. Multiplying the equation (3) corresponding to the air domain (without magnetization source term), with the elementary solution $u^* = 1/4\pi r$ of the *Laplace* equation and integrating it over the whole free space, as in [6], we obtain, after several operations [6], the discrete system equations of BEM:

$$\begin{bmatrix}H_x&0&0\\0&H_y&0\\0&0&H_z\end{bmatrix}\begin{Bmatrix}A_x\\A_y\\A_z\end{Bmatrix}+\begin{bmatrix}G_x&0&0\\0&G_y&0\\0&0&G_z\end{bmatrix}\begin{Bmatrix}\partial A_x/\partial n\\\partial A_y/\partial n\\\partial A_z/\partial n\end{Bmatrix}=\begin{Bmatrix}F_{0x}\\F_{0y}\\F_{0z}\end{Bmatrix}, \tag{15}$$

or:

$$[H]\{\mathbf{A}\}+[G]\{\partial A/\partial n\}=\{F_0\}\,. \tag{16}$$

Multiplying with $[G]^{-1}[D]$ the last equation, it becomes:

$$[D][G]^{-1}[H]\{\mathbf{A}\}=-[D]\{\partial A/\partial n\}+[D][G]^{-1}\{F_0\}\,. \tag{17}$$

The matrix equations (13) and (17) are coupled using the relation (6):

$$[P+K]\{\mathbf{A}\}=[D][G]^{-1}\{F_0\}+[\overline{\overline{S}}]\{\mathbf{M}\} \tag{18}$$

with: $[K]=1/2([K_B]+[K_B]^T)$, $[K_B]=[D][G]^{-1}[H]$ and $[\overline{\overline{S}}]=\begin{bmatrix}0&S_{12}&S_{13}\\S_{21}&0&S_{23}\\S_{31}&S_{32}&0\end{bmatrix}$,

where:

$$S_{12_{kj}}=\int_{\omega_j}\nabla N_k(-\mathbf{k})d\Omega=-S_{21_{kj}},\quad S_{23_{kj}}=\int_{\omega_j}\nabla N_k(-\mathbf{i})d\Omega=-S_{32_{kj}},\quad S_{31_{kj}}=\int_{\omega_j}\nabla N_k(-\mathbf{j})d\Omega=-S_{13_{kj}}$$

The nonlinear equation is solved, through a fixed-point procedure described below. The algorithm of the method is as follows:

1) We start with initial condition for magnetic field $B^0 = 0$ and sources $J^0=0$ and an arbitrary value for M^0;
2) Nonlinear iteration step $i = 1$ is performed (then i incremented) ;
3) From solution of system (18), the magnetic flux density inside each element is computed at iteration i;

4) The error in comparison with the exact solution in terms of magnetic flux density B^* for the current iteration i is evaluate using the norm described in [1]:

$\left\| B^* - B^i \right\|_V \le \frac{1}{1-\theta} \left\| \Delta\mu_0 M^i \right\|_V$, with θ being the contraction factor defined as in [2];

if the error is less than an imposed value, we exit the nonlinear iteration cycle, otherwise we follow the nonlinear iterations (jump to 2);

System (18), having the coefficient matrix partially banded and symmetric, is solved using the active column solver based on Gauss elimination method [6].

4. Sensitivity analysis

We used the FEM-BEM code described in the previous section to simulate the static field problem of a yoke with sample. The yoke is equipped with two exciting coils and it is used to magnetize the sample. The region in the welded specimen affected by heating is modeled as a ferromagnetic part, because ferrite inclusions are present there. For our problem, we only consider a reduced zone for modeling the specimen. The specimen thickness is 25 mm. The specimen contains a crack, ranged within 3 to 9 mm length, 20% to 80 % depth and having 0.5 mm width. In Fig. 1 are shown the overall dimensions of yoke and specimen used in this simulation. Figure 2 shows *(a)* the nonlinear magnetic yoke and specimen used in this simulation. Figure 2 shows *(a)* the nonlinear magnetic characteristic of the yoke and *(b)* the nonlinear characteristic for specimen material. The exciting coils are cylindrical, with R_{min} = 11 mm, R_{max} = 46 mm, H = 35 mm, each of them carrying I_{tot} = 2000 AT and being placed on the two columns of the yoke.

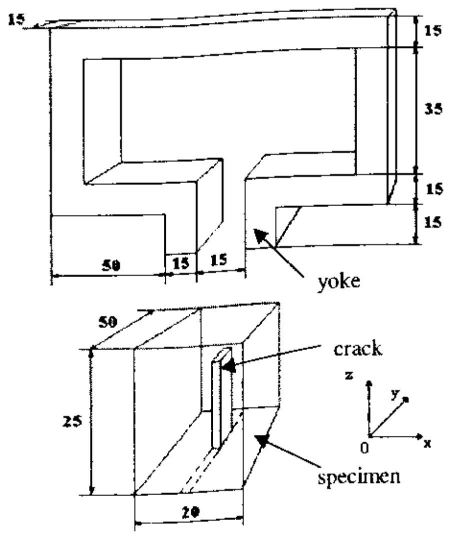

Fig. 1 The simulated experimental device, with yoke and specimen dimensions (given in mm)

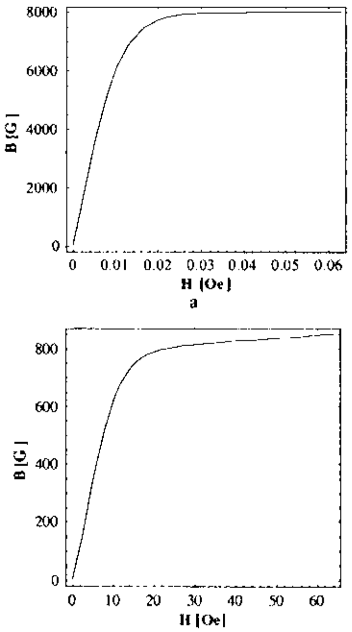

Fig. 2 B-H characteristic for: (a) yoke and (b) the specimen material

The x-component of magnetic flux density along a line in y-direction, centered, with constant liftoff was computed in 21 equally spaced points 1 mm apart. In the real experiment, Hall sensors must be used for measuring the field, which is largely over 1 G, *i.e.* TFG sensors did not represent a valid option to be used. The difference field, comparing with the case without crack, is computed.

The difference signal is defined as difference between signal in the case of specimen with crack and the signal in the case without crack. Figure 3, a) shows the variation of the difference signal ΔB_x, with the crack depth for outer defects (OD) 0.5 mm width, 7 mm length, 20 %, 40 %, 60 % and 80 % depth. In Fig. 3, b, the dependence of the difference signal ΔB_x on the crack length for a 0.5 mm width, 40 % OD crack is shown. In Figure 4, a, the variation of the difference signal ΔB_x with the crack depth for an 0.5 mm width, 7 mm length, ID crack is shown. Results for 20 %, 40 %, 60 % are presented. In Figure 4, b, the dependence of the difference signal ΔB_x on the crack length for a 0.5 mm width, 40 % ID crack is shown.

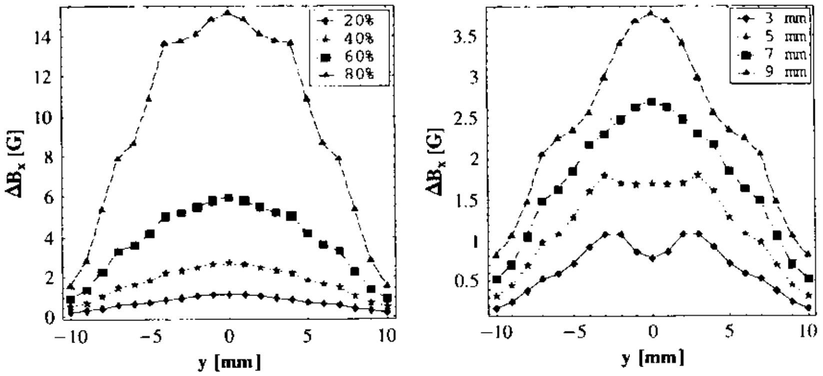

Fig.3 Difference signal ΔB_x variation for an 0.5 mm width, OD crack a) with the crack depth for a 7 mm length crack; b) with the crack length for a 40 % depth crack.

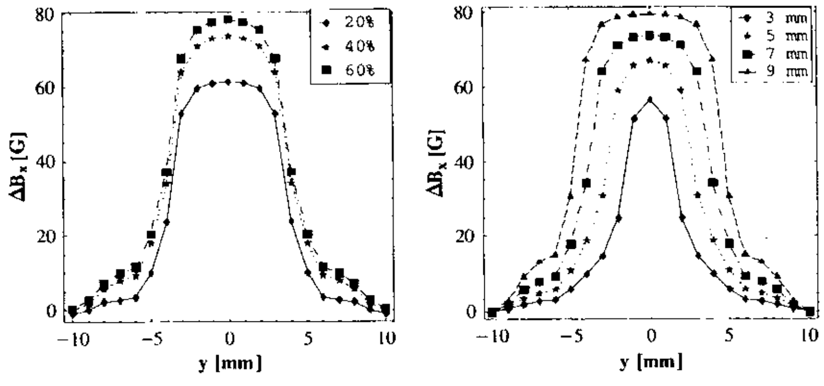

Fig.4 Difference signal ΔB_x variation for an 0.5 mm width, ID crack a) with the crack depth for a 7 mm length crack; b) with the crack length for a 40 % depth crack.

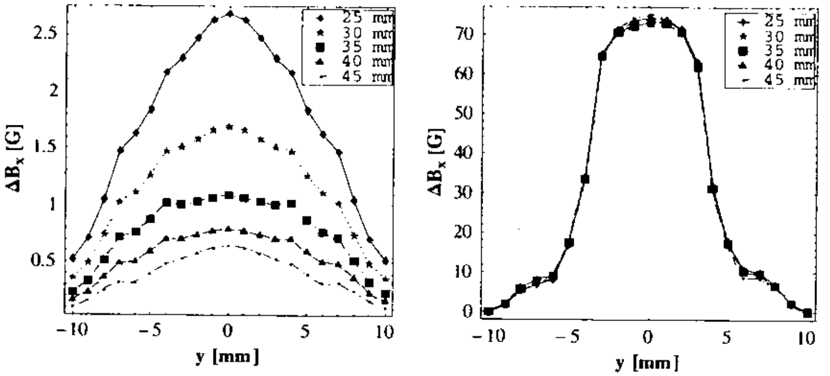

Fig.5 Difference signal ΔB_x variation with specimen thickness for an 40 % depth, 0.5 mm width, 7 mm length crack a) for an OD crack; b) for an ID crack; values for 25, 30, 35, 40 and 45 mm thickness of the specimen.

Fig. 5 shows the difference signal variation with specimen thickness, for values of thickness ranged between 25 and 45 mm, both for OD and ID cracks.

From this plots we can see that even for 20% OD cracks, 3 mm length, the difference signal still can be emphasized. In the next section we explain about the strategy used for reconstructing from this signals the crack parameters.

5. Inverse mapping of the scanned magnetic flux density values

The proposed reconstruction algorithm is based on a statistical regression of the inverse mapping signal to defect parameters. A multi-level-resolution representation of the input-output relationship was introduced. This is realized by the combination of two modules: the statistical analysis and transformation of the input data - by Principal Component Analysis (PCA) -, and the NN with incremental-resolution learning [5][7]. The first module discovers the principal directions (features) of data variances and rotates the original coordinate axes along these directions, eliminating the multicolinearities of the data set. As for the second module, the network contains a single hidden layer, and additional direct connections between inputs and outputs to account for the mapping linearities. The training starts with only one hidden node, and for each training epoch a new node is created, the new input-hidden connections receive random weights and the rest of the weights are solved by a least-square minimization using singular value decomposition. The over-determined equation system is:

$$\left[\mathbf{A} \quad f_1(\mathbf{A}\cdot\mathbf{W}_{ih})\right]\cdot\begin{bmatrix}\mathbf{W}_{io}\\ \mathbf{W}_{ho}\end{bmatrix} = f_2^{-1}(\mathbf{B}), \tag{19}$$

where **A**, **B** represent the input, and output training sets, respectively the f_1 and f_2, the nonlinear activation functions for the hidden and output nodes, $\mathbf{W}_{ih}$ is a randomly generated, fixed coefficient matrix and $\mathbf{W}_{io}$, $\mathbf{W}_{ho}$ are the matrices containing the unknowns, *i.e.* the input-output and the hidden-output interconnections weights, respectively. Three sets of data are used, for training, validation and verification. The validation set is used only to control the training optimality, by monitoring the currently achieved estimation error. The verification set is used only in reconstruction and, if available, the corresponding 'true" defect shapes are compared with the estimated ones. At this stage, the previously recorded

files are employed and only elementary operations are required for data transformation and propagation through the trained network. Therefore, this procedure is very fast, allowing a real-time implementation with small computational demands during the actual testing. Being based on the learning an input-output mapping from a set of examples (the training set) or fitting in a least-squares sense a hypersurface of this set in view of acquiring good generalization properties in unpopulated points, the overall procedure is equivalent to a statistical regression. As the training set covers only a small part of the parameter space, the generality of the training set is obtained by random generation of the crack parameters.

The defect is represented using a cell parameterization, to each cell, having -1 or 1 value, corresponding a material or crack sub-domain. The signals are associated with the input nodes and defect parameters with the output nodes of the neural network.

6. Reconstruction of crack shape

Crack reconstruction from simulated signals is furthermore investigated. A database containing 200 cases in the training set, 30 in the validation set and 20 in the verification set, was computed. Only OD cracks, 0.5 mm width, 20% to 80 % depth, with irregular, randomly generated, open profile were used for training. All cracks were modeled inside a 9 x 5 cells box each with 1mm × 0.5 mm × 5 mm dimensions, centered under the scan line. The number of scan points is 21 and only the x-component of magnetic field along the y-axis oriented scan line is used. Therefore, the number of output nodes is 45, the number of input nodes is equal to 21. For testing the effectiveness of this procedure also in the case of noise polluted data, the data sets were also polluted with 10% and 20% artificial white noise. The two levels of artificial noise were injected equally in the verification set and in the training set. Therefore, three different results are available. The first set, reconstructions after training with noise-free simulated data from noise-free signals (see Fig.6, b). The second set, after training with additional 200 cases, 10% polluted, reconstructions from signals polluted with 10 % noise (see Fig. 6, c). The third set, after training with additional 400 cases, 200 polluted with 10% white noise and another 200 polluted with 20 % white noise, reconstructions from signals polluted with 20 % noise (see Fig.6, d). Average deviations error is bellow 10 %. Training is stopped after an average value of 250 epochs. The added noise in the training set is used traditionally in NN community for avoiding the overfitting. In our case, this also allows the network to learn from noise-polluted signals. Although the validation error has large values, the learning evolve toward very small values of learning errors and some good reconstructions are obtained (see in Fig. 6,a, comparison with true profile of the crack).

7. Conclusions

The work emphasized in this material contributes to two aspects of the research concerning nondestructive testing techniques with static fields. First, a 3D code for nonlinear static field was developed. The sensitivity analysis shows a good resolution of signal even for small cracks. Second, the reconstruction using an auto-adaptive Neural Network training algorithm give good approximation of crack parameters, even for a reduced training set. The use of a PCA module, before presenting the data to the network, eliminates the multicoliniarities in the data set, reduces the ill-posedness of the inverse mapping to be reconstructed, representing thus a regularization factor. Increased quality of the reconstruction is possible using additional regularization methods.

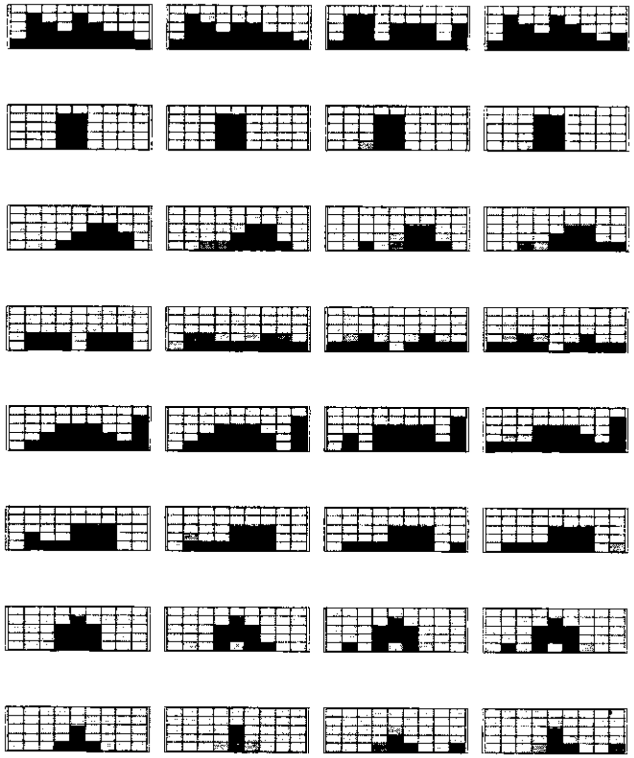

a b c d

Fig. 6 Comparison between a) true shape of cracks; and reconstructed results for b) noise-free signals data after training with noise-free database; c) 10% polluted signals after training with additional training set noise polluted with 10% white noise; d) 20% polluted signals after training with additional training set noise-polluted with 10% white noise and 20% white noise. Basic data sets were 200 for training, 30 for validation and 20 for verification sets. Average deviations error is bellow 10 %.

References

[1] R. Albanese, F.I. Hantila and G. Rubinacci, A Nonlinear Eddy Current Integral Formulation in Terms of a Two-Component Current Density Vector Potential, *IEEE Trans. on Magn.*, no. 3, pp.784-787, 1996.

[2] F.I. Hantila, G. Preda and M. Vasiliu, Polarization Method for Static Fields, *in Proc. of 12th COMPUMAG, Sapporo*, Oct. 25-28, 1999, pp.664-665.

[3] J. Fetzer, S. Kurtz and G. Lehner, Comparison of analytical and numerical integration techniques for the boundary integrals in the BEM-FEM coupling considering TEAM workshop problem no. 13, *IEEE Trans. on Magn.*,Vol. 33, no. 2, pp.1227-1230, 1996.

[4] S. Kurtz, J. Fetzer and G. Lehner, A novel iterative algorithm for the nonlinear BEM-FEM coupling method, *IEEE Trans. on Magn.*, Vol. 33, no. 2, pp.1772-1775, 1997.

[5] C.L.P.Chen, A Rapid Supervised Learning Neural Network for Function Interpolation and Approximation, *IEEE Trans Neural Networks*, Vol. 7, 1996, pp.1220-1230.

[6] Z. Chen and K. Miya, ECT Inversion Using a Knowledge-Based Forward Solver, *J. Nondestr. Eval.*, Vol. 17, No. 3, 1998, pp. 167-175.

[7] R.C.Popa and K.Miya, Approximate inverse mapping in ECT, based on aperture shifting and neural network regression, *J. Nondestr. Eval.*, Vol. 17., No. 4, 1998, pp. 209-221.

Electromagnetic Nondestructive Evaluation (V)
J. Pávó et al. (Eds.)
IOS Press, 2001

A Multilayer Perceptron Approach to a Non-Destructive Test Problem

P. BURRASCANO, E. CARDELLI, A. FABA, S. FIORI, A. MASSINELLI
Dept. of Industrial Engineering, University of Perugia – Perugia
Via Duranti 1-A/4, Perugia (Italy)

Abstract. The aim of this paper is to present a neural-network based solution to a non-destructive test problem, namely the identification of the diameter of a cylindrical defect, on a metallic slab, by means of multi-layer perceptron based modeling of the complex interaction between the metallic slab and the electromagnetic probe. We propose to train a network by means of a consistent data-set obtained by real-world (measured) data, labeled with the defect diameters, and to successively apply the learnt network to the estimation of the dimension of a set of unknown defects.

1. Introduction

Optimization techniques are frequently applied to the most important processes in the industry, obtaining greater economical benefits by improving quality and increasing productivity. The basis for success of these techniques is the availability of the system model. However, it is often difficult to obtain an accurate representation, due to the inherent non-linearity, complexity and uncertainty of the industrial processes.

Unlike the traditional mathematical identification approaches, neural network based modeling enables us to generate a reasonable model without demanding a detailed knowledge about the physical relationships of the underlying phenomena (as demonstrated, for instance, by Hornik and Stinchcombe, Haykin, and Fiori [11,12,13]). This reduces the complexity of the modeling task. In fact, artificial neural networks are known to perform universal function approximation, provided that the right network topology is chosen and a sufficiently large set of examples of the function to be approximated is available (for a modern review see Haykin and Bishop [3,12]). Such ability may be advantageously employed in those practical applications where the exact model of a physical system is too difficult to derive or to handle with, and an amount of measures intrinsically describing the behavior of such a system are available; in this case neural networks provide a black-box data-based model of the observable part of the system.

Artificial neural networks have recently found widespread applications in diverse areas as a practical tool for modeling, simulation, control, and prediction. Especially prevalent in the applications are the multi-layer perceptron (MLP) networks, which are typically trained with data or patterns collected during actual operations; after a